

A comparative analysis of powder ENDOR spectra of aromatic and aliphatic radicals by exact and 1st order simulation

Roland Erickson^{a,b}, Anders Lund^{a,*}

^a Department of Physics, Chemistry and Biology, Linköping University, S-581 83 Linköping, Sweden

^b FMV, Box 13400, S-580 13 Linköping, Sweden

ABSTRACT

Exact and perturbation methods were employed in simulations of powder ENDOR spectra to obtain the anisotropic hyperfine (*hfc*) and nuclear quadrupole (*nqc*) coupling constants of certain organic radicals of interest in fundamental research and in applications in radiation research, surface chemistry and biophysics. The principal *hfc* values of the ring protons and methyl substituents for several aromatic cations trapped in disordered matrices might be more accurate than those previously reported using regular EPR. Only one of the earlier assignments of the naphthalene cation spectrum was in acceptable agreement with the simulations. The proton couplings at the β -position of alkyl radicals were deduced by simulations while the spectrum due to α -couplings with appreciable anisotropy was weak. Accurate simulation of the ^{14}N ($I = 1$) spectra in bio-radicals was obtained by adjustment of the relative orientation of the principal *hfc* and nuclear quadrupole coupling (*nqc*) tensors as well as the principal values. Adjustment of the excitation width parameter employed in the software was also required in a few cases to improve the agreement with the experimental spectra. The *hfc* patterns due to matrix nuclei (^1H and ^7Li) around the radicals of X-irradiated samples were simulated to elucidate the nature of the trapping sites in materials used for EPR dosimetry. ENDOR simulation programs known to us are presented in an Appendix. The performance of the ENDORF2 program used in previous works was examined by comparison with exact treatment. Input and output examples, source and executable codes used in this work can be downloaded at <https://github.com/EndorF2/Simulation>.

1. Introduction

The electron nuclear double resonance (ENDOR) technique provides a method to determine the weak hyperfine couplings (*hfc*) that are not resolved by regular EPR in radicals and similar species [1]. The ENDOR spectra are commonly simple in solutions and single crystals and may be interpreted without simulation. The spectra of disordered solids ('powders') are often broad, however, and the anisotropy of the *hfc* tensors can produce complex line shapes. The intensity is also affected by several phenomena like hyperfine enhancement, magnetic relaxation and angular selection further considered below, as well as instrumental factors contributing to the complexity of the line shape. It has therefore been difficult to accurately determine the magnitude and anisotropy of the couplings from the observed spectral features of powders without performing simulations.

The ENDOR spectrum originates from a single position in the EPR spectrum, since the magnetic field is kept constant in the experiment, and in a powder sample the EPR resonance condition is met only for a certain range of orientations.¹ This is opposite to the EPR spectrum which is a superposition of spectral intensities from all possible

orientations. Computer simulations commonly take in account the *hfc* anisotropy, the hyperfine enhancement and the angular selection, sometimes also the *nqc* (nuclear quadrupole coupling) anisotropy for nuclei with $I \geq 1$, but less frequently the magnetic relaxation. Paired with other electron magnetic resonance (EMR) methods and the chemical and physical knowledge of the species, ENDOR simulations facilitate the determination of the *hfc*- and, for $I \geq 1$, *nqc* -tensors.

Several powder ENDOR simulation methods, including appropriate theory, have been described in the literature. ENDOR transition frequencies were calculated by taking the difference between appropriate eigenvalues of the spin Hamiltonian involved, using perturbation theory methods [2–10] or exact diagonalisation of the spin Hamiltonian [11–18]. But whereas transition intensities in EPR could often be predicted in good agreement with experiment, simulation of ENDOR intensities often showed poorer agreement. ENDOR transition moments are affected by a number of factors. Theories to account for the hyperfine enhancement, angular selection, and the distribution of orientations of the resonant paramagnetic species relative to the radio frequency (RF) field have been developed and are commonly incorporated in simulation software for solid state ENDOR spectra. The simulation software

* Corresponding author.

E-mail address: anders.lund@liu.se (A. Lund).

¹ This is valid when the electron spin–spin cross relaxation rate is much slower than the electron spin–lattice relaxation rate, so that only the EPR transitions located at the field setting are brought into resonance by the microwaves.

packages for solid state ENDOR currently known to us mostly ignore spin relaxation, however. A model of relaxation in solution ENDOR has been worked out by Freed and co-workers [19], which has been extended by Brustolon et al. to the $^{\circ}\text{OOC-}\dot{\text{C}}\text{H-COO}^{\circ}$ radical at room temperature in γ -irradiated single crystal KH malonate [20] and Clarkson et al. [5,6] have applied a theory, developed by Dalton and Kwiram [4], to the powder ^1H ENDOR spectra of perylene radical cations generated on silica-alumina catalysts. None of the other simulation software packages for solid state ENDOR [4–18] seem to have included relaxation effects. The detailed knowledge of all, in general anisotropic, relaxation rates needed in a theoretical model makes the calculations complex and may be difficult to elucidate in powders, and only a few experimental investigations have been made of relaxation in ENDOR of solid samples at low temperatures [20b-c]. The neglect of relaxation in simulations may contribute to the discrepancies between simulated and experimental ENDOR intensities observed. However, the use of exact or first order instead of zeroth order or constant transition probabilities, and angular selection to predict intensities, while neglecting relaxation, can still in many cases give a sufficiently good fit to facilitate a spectral interpretation in powders, as demonstrated e.g. in Refs. [2,3,8,9].

Methods to compute ENDOR signals from transition metal complexes obtained at arbitrary field positions have been developed in several works [7,21,22]. Orientation selectivity was taken in account, but ENDOR probabilities were not computed. Kreiter and Hüttermann [12] have described a general theory to calculate the powder ENDOR spectra due to *hfc* and *nqc* constants. Magnetic energies and wave functions were calculated by exact diagonalization of the spin Hamiltonian while ENDOR transition probabilities were computed to zeroth order, neglecting hyperfine enhancement effects. A similar theory, but incorporating first order transition probabilities, has been described by Keijzers et al. [11]. A general treatment for the simulation of ENDOR spectra in solids has been developed by Stoll and Schweiger [15–17]. The transition frequencies were calculated by exact diagonalisation of the spin Hamiltonian, the intensities [23] were obtained in a similar way as by Keijzers. The theory is implemented in the Matlab software EasySpin [17]. An option to calculate frequencies using the perturbation theory by Iwasaki [24] was included in EasySpin, but the allowed transition intensities were set equal to one and were not computed.

Though several software packages have been developed for the simulation of powder ENDOR spectra of free radicals [2–18], comparisons of results obtained by different methods have, to our knowledge, not been extensively made. In this work simulations were performed employing exact diagonalisation of the Hamiltonian for both energies and intensities [15–17] of powder ENDOR spectra of free radicals previously simulated mainly using perturbation theories, in systems of interest in radiation research, surface chemistry, biochemistry and related fields. Comparisons with experimental data and simulations employing perturbation theory were presented. The performance of the ENDORF2 program [8,9] for the calculation of ENDOR spectra due to nuclei with arbitrary spins was examined. The transition energies and moments, calculated by a perturbation treatment with arbitrary relative magnitudes of the *hfc*, nuclear Zeeman, and *nqc* ($I \geq 1$) terms, were in excellent agreement with those computed with exact theory. Simulations with EasySpin [17] were performed to validate the data obtained for aromatic and aliphatic radicals, radicals with *hfc* and *nqc* splittings due to nuclei with $I \geq 1$ and for matrix and ligand nuclei. The influence of the excitation width parameter employed in [17] and the corresponding convolution parameter in [8,9] was examined.

2. Theoretical methods

The ENDORF2 software is based on a first order treatment of the spin Hamiltonian, originally applied for the analysis of EPR spectra of free radicals with large nuclear quadrupole coupling (*nqc*) due to nuclei with $I \geq 1$ [25]. The theory differs from other perturbation schemes, which assume *nqc* terms to be much smaller than the *hfc* interaction, or are

neglected [23,24,26]. An anisotropic $S=\frac{1}{2}$ system containing an arbitrary number (n) of nuclei was considered, Eq. (1).

$$H = \mu_B \mathbf{B} g \mathbf{S} + \sum_{i=1}^n \mathbf{I}_i A_i \mathbf{S} + \mathbf{I}_i Q_i \mathbf{I}_i - \mu_N \sum_i^N \mathbf{B} \cdot \mathbf{I}_i \quad (1)$$

Assuming that the electronic Zeeman term is dominant, while the relative magnitudes of the hyperfine and nuclear terms are arbitrary, the perturbation operator consisting of the *hfc*, *nqc* and nuclear Zeeman interactions for each nucleus (j) with $I_j \geq 1$ is then given by (2).

$$H_j' = \mathbf{I}_j A_j \mathbf{u} \mathbf{S}_u + \mathbf{I}_j Q_j \mathbf{I}_j - \mu_N \sum_i^N \mathbf{B} \cdot \mathbf{I}_i \quad (2)$$

The unit vector $\mathbf{u} = g\mathbf{B}/|g\mathbf{B}|$ is along the effective field direction, the other symbols have their usual meaning. A detailed definition can be found in [8]. The theory was extended in [8,9] to calculate single crystal or powder ENDOR spectra of $S = \frac{1}{2}$ species with *hfc* and *nqc* interactions. ENDOR transition energy and moment formulas were derived. No restrictions on either relative magnitude or orientation were imposed on the *hfc*, *nqc*, and nuclear Zeeman terms, except that they must be much smaller than the electron Zeeman interaction [8,9]. The method has been implemented in the simulation program ENDORF2, DOI <https://doi.org/10.5281/zenodo.4670928> available on github <https://github.com/EndorF2/Simulation/tree/v1.0>.

2.1. ENDOR transition frequencies

The ENDOR transition frequency between two nuclear eigenstates $|h_j\rangle$ and $|k_i\rangle$ of the same electronic state, m_S , $\Delta m_S = 0$, is obtained from Eq. (3), using the eigen-energies of the perturbation Hamiltonian (2).

$$\nu_{h_j k_i} = |E'(h_j) - E'(k_i)| \quad (3)$$

Note that in general the eigenstates $|h_j\rangle$ and $|k_i\rangle$ are mixtures of nuclear spin states. $E'(h_j)$ and $E'(k_i)$ are the nuclear energies of the two states, calculated by diagonalisation of the spin Hamiltonian (2). A first order treatment is justified in X-band spectra for *hfc* smaller than 40–60 MHz, unless other interacting nuclei with very large *hfc* [10] are also present. For cases incorporating larger couplings the second order corrections in [10,24] can be applied. However, they were not implemented in the ENDORF2 program, since the major application was to measure small *hfc* splittings that are unresolved in the EPR spectra. Simulated ENDOR frequencies of nuclei incorporating *hfc* up to 60.8 MHz in the tyrosyl free radical, were thus shown to agree within 0.1 MHz with experimental observations, using the proton *hfc* parameters in ribonucleotide reductase from Escherichia coli [27]. An additional second-order effect occurs for magnetically equivalent nuclei where cross terms may split the basic, first order ENDOR frequency into several transitions. The second-order splitting might be noticeable for larger *hfc* measured in single crystals. Splittings or shifts of up to 0.2 MHz have been observed by Toriyama and coworkers for methyl protons with a *hfc* of ca 60 MHz [28]. For smaller *hfc* these are generally too small to be resolved in broad powder ENDOR lines. For the four equivalent protons of the naphthalene cation, described in [3] and Table 2, the largest second-order splitting is ca. 0.023 MHz occurring for a *hfc* tensor component of -7.9 MHz. Since the linewidth is 0.6 MHz the splitting is not resolved. These splittings were not taken in account in Eq. (3), but the second order correction formulas proposed in [28] can be applied for the larger *hfc* couplings of aliphatic radicals, if necessary.

2.2. ENDOR transition probabilities

The probability for a radiation induced transition between nuclear spin states $|h_j\rangle$ and $|k_j\rangle$, $\Delta m_S = 0$, for a nucleus j with spin I_j , is given by Fermi's golden rule [28].

$$P = 2\pi W^2 \rho(\omega) \quad (4)$$

Table 1

First order formulas for ENDOR transition probabilities, W^2 , in multiples of $(B_2/B)^2$ in a single crystal for a transition between nuclear states $|a\rangle \leftrightarrow |b\rangle$, $\Delta m_s = 0$ of a nucleus with spin I , for different conditions on \mathbf{A} , \mathbf{Q} , \mathbf{g} and orientation of \mathbf{B} and \mathbf{B}_2 . Equation (6), listed as case (a), and used in the ENDORF2 program, is valid for hfc , nqc , and nuclear Zeeman interactions of arbitrary relative magnitudes, while assuming the electronic Zeeman term is dominant, and modest g-anisotropy. Neglecting nqc the formula in case (a) simplifies to the formula in case (b), which agrees with an expression first derived by Toriyama et al. [28]. In the special case of when the external fields \mathbf{B} and \mathbf{B}_2 are parallel to principal axes \mathbf{i} and \mathbf{j} of \mathbf{A} , and \mathbf{g} is isotropic the formula in (a) simplifies to case (c), which agrees with expressions published in [23,28,30]. Neglecting nqc splittings, but allowing large g-anisotropy, Schweiger and Günthard [23] have derived a very accurate formula, given in our notation as case (d). If $\mathbf{rgg} \ell/g^2$ -terms are neglected the formula is identical with the formula in case (b).

Case	Conditions	W^2 , in multiples of $(B_2/B)^2$	Ref.
(a)	Arbitrary \mathbf{A} , \mathbf{Q} Modest g-anisotropy	$ \langle a \mathbf{ICr} b\rangle ^2$	[8]
(b)	$\mathbf{Q} = 0$ Arbitrary \mathbf{A} Modest g-anisotropy	$f_{\pm}^2[\mathbf{rCCr} - (\mathbf{rCC} \ell)^2/(\ell \mathbf{CC} \ell)]$	[9,10,23,28]
(c)	$\mathbf{Q} = 0$ $\mathbf{B} \parallel$ principal axis \mathbf{i} $\mathbf{B}_2 \parallel$ principal axis \mathbf{j}	$f_{\pm}^2 \nu_N^2 [1 - m_s A_j/\nu_N]^2$	[9,10,23,28,30]
(d)	Isotropic \mathbf{g} $\mathbf{Q} = 0$ Arbitrary \mathbf{A} , \mathbf{g}	$f_{\pm}^2[\mathbf{rCCr} - (\mathbf{rC} \ell)^2 + (\mathbf{rC} \ell \cdot \mathbf{rgg} \ell \times \nu_N/g^2)^2 - (\mathbf{rCC} \ell \cdot \mathbf{rgg} \ell \times \ell \mathbf{C} \ell \times \nu_N/g^2)^2/(\ell \mathbf{CC} \ell)]$	[23]
Notation: $\mathbf{C} = m_s \mathbf{Ag}/g - \nu_N \mathbf{1}$ $f_{\pm}^2 = [(I+1) \cdot m_l(m_l \pm 1)]/4$			
Formulas for W^2 when $\mathbf{Q} = 0$, cases (b)–(d), apply to $ a\rangle = m_l \pm 1\rangle$, $ b\rangle = m_l\rangle$. Wave functions $ m_l\rangle$ are eigen-functions of the operator $I_k = \mathbf{I} \cdot \mathbf{k}$ where $\mathbf{k} = \mathbf{C} \ell / \mathbf{C} \ell $.			

where $\rho(\omega)$ is the frequency distribution function of the radiation. The transition probability (5) selects the allowed transitions and predicts the relative intensities, neglecting relaxation effects.

$$W^2 = |\langle \Phi(m_s, h_{1...h_{j-1}}, h_j, h_{j+1}, \dots, h_n) | \mathbf{B}_2 (\mu_B \mathbf{gS} - \sum g_j \mu_j^N \mathbf{I}_j) | \Phi(m_s, h_{1...h_{j-1}}, k_j, h_{j+1}, \dots, h_n) \rangle|^2 \quad (5)$$

In Eq (5) $h_{1...h_{j-1}}, h_{j+1}, \dots, h_n$ are the nuclear eigenstates of the $n-1$ nuclei that remain unchanged in the ENDOR transition, whereas the nuclear eigenstate of nucleus j changes from h_j to k_j . The theory developed in [8,9] used first-order eigenfunctions to predict ENDOR transition probabilities properly. First order probabilities show good performance, whereas zeroth-order formulas may differ from exact values by orders of magnitude, as described by Schweiger and Günthard [23]. Zeroth-order transition probabilities only show orientation dependence when the static field is oriented away from the principal axes of the hfc tensor and are insufficient to predict hyperfine enhancement effects. An example of the resulting difference in simulated intensities using zeroth and first order transition probabilities is discussed in section 3.3, for ^{14}NO -ligated ferrocycytochrome c -heme a_3 . The transition probability derived in [8,9] for the transition between the nuclear states $|h\rangle$ and $|k\rangle$ of a nucleus with spin I , with first order wavefunctions, is given by Eq.(6), dropping the nuclear index j in Eq. (2) to simplify the formula.

$$W^2 = (B_2/B)^2 |\langle h|\mathbf{ICr}|k\rangle|^2 \quad (6)$$

The Hamiltonian operator used in (6) represents the coupling between the RF-field, \mathbf{B}_2 , and the electron and nuclear magnetic moments. The RF-field, $\mathbf{B}_2 = B_2 \mathbf{r}$, oriented along the unit vector \mathbf{r} , is perpendicular to the static field in conventional ENDOR spectrometers. The quantity \mathbf{C} in (6) is the “ENDOR tensor”.

$$\mathbf{C} = m_s \mathbf{Ag}/g - \nu_N \mathbf{1} \quad (7)$$

where \mathbf{A} is the hfc matrix, $\mathbf{1}$ the identity matrix, and ν_N the nuclear Larmor frequency.

Equation (6) applies for free radical systems containing nuclei with arbitrary I , including $I \geq 1$ having hfc , nqc , and nuclear Zeeman interactions which may be of comparable magnitudes.

Eq. (6) is listed in Table 1 as Eq. case (a), together with formulae neglecting nqc , cases (b–d). With zero nqc Eq. (6) can be simplified to an analytical formula, Eq. case (b) of Table 1, first reported by Toriyama et al. [28]. The formulas in [4] were derived under similar assumptions. Without nqc the nuclear spins are quantised along the unit vector $\mathbf{k} = \mathbf{C}\ell/|\mathbf{C}\ell|$. Here ℓ is a unit vector in the direction of the static field. The nuclear wavefunctions are then eigenstates $|m_l\rangle$ of the operator $I_k = \mathbf{I} \cdot \mathbf{k}$. Eq. cases (a) and (b) assume that the g-anisotropy is modest so that the relation $(1/g^2)\mathbf{rgg} \ell \ll 1$ is valid. The left part may be recognised as the dot product of the unit vectors along the effective RF and the static magnetic field, yielding a value for the angle between these vectors. In conventional spectrometers the RF-field direction \mathbf{r} is perpendicular to the static field direction ℓ . The relation is then fulfilled for most free radicals since their g-anisotropy amounts only to a few percent of the isotropic value.

Neglecting nqc splittings, but allowing large g-anisotropy, Schweiger and Günthard [23] have derived a very accurate formula, given in our notation as Eq. (d) in Table 1. The equation shows perfect agreement with exact numerical calculations even for g-anisotropies exceeding 30% of the isotropic value. If $\mathbf{rgg} \ell/g^2$ -terms are neglected the equation is identical with Eq. (b). For g-anisotropies up to a few percent these terms have negligible effect. For a larger anisotropy of 10 % Eq. (b) is, as a rule of thumb, accurate to within 1–2% of the more exact value of Eq. (d). The relative difference between the two equations for a case of a methylene proton in Cu(II)-doped α -glycine, with \mathbf{g} and proton hfc tensors $\mathbf{g} = (2.0434, 2.0715, 2.2644)$ and $\mathbf{A} = (6.35, 1.99, 1.14)$ MHz [31], varied from 0.4% up to 1.5% of the ‘exact’ value, for twelve transitions calculated for different combinations of \mathbf{B} and \mathbf{B}_2 parallel to either of the crystal axes \mathbf{a} , \mathbf{b} and \mathbf{c}^* [10]. The largest discrepancy of 1.5% occurred for the $m_s = +1/2$ transition with \mathbf{B} along crystal axis \mathbf{b} and \mathbf{B}_2 along \mathbf{a} [10].

The intensities of the ENDOR lines, calculated with Eq. (6), were previously found to vary depending on the orientation of the RF field in single crystal [8]. A similar variation was observed in this work, using EasySpin [15–17] to compute the intensities of the four ^{14}N transitions of the $\text{CH}_2\text{NHCOC}_6\text{H}_5$ radical fragment as a function of the RF-field orientation in the bc crystal plane of hippuric acid. The calculated ratios, I:II:III:IV = 0.137:0.116:0.395:0.352, obtained with the RF-field \mathbf{B}_2 along the crystal c -axis deviated significantly from the values 0.122:0.159:0.333:0.385 with \mathbf{B}_2 along the b -axis.

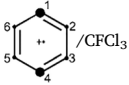
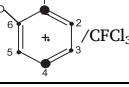
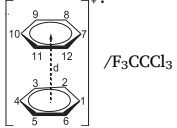
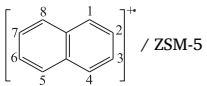
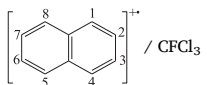
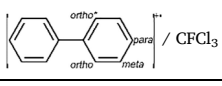
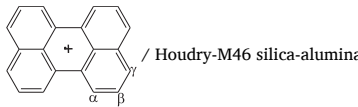
As indicated in Fig. 1 the intensity ratios obtained with EasySpin and ENDORF2 for the same orientation of the RF field agreed very well, however. The static field was aligned along the crystallographic a -axis, the RF-field was at an angle ψ with crystal axis c . The calculations indicate that the transition moments computed with Eq. (6) are close to the exact ones, even in the presence of a substantial nqc interaction, under the prevailing condition of a dominating electron Zeeman term with small g-anisotropy. This conclusion was further supported by the close similarity of the single crystal spectra in Fig. 2, obtained by exact calculation [17] and by the 1st order treatment in [8]. Similar spectra obtained with ENDORF2 were previously used to help interpret the powder spectrum [8].

2.3. The ENDOR powder lineshape

The first derivative line shape at the frequency ν and static magnetic field B is modelled by the formula (8), ignoring spin relaxation and instrumental effects [8,9].

Table 2

^1H hyperfine coupling tensors of aromatic cation radicals determined by spectrum simulation of powder ENDOR spectra. The two α Euler angle values denote the different orientations of two symmetry related tensors (unstarred, and starred * respectively) with equal principal values.

Structure / Matrix	Hfc tensor	Principal values (MHz)			Euler Angles ($^\circ$)			Ref.
		x	y	z	α	β	γ	
 / CFCl_3	A_1, A_4 A_2^*, A_5^*, A_3, A_6	-38.8 -8.4	-11.1 0.0	-26.0 -7.9	0 -67.8*/-112.2	0 0	0 0	[36]
 / CFCl_3	A_1, A_4 $A_2^*, A_5^*, A_3, A_D = A_3/6.54$	-38.3 -8.2	-10.8 0	-25.9 -8.2	0 -67.8*/-112.2	0 0	0 0	[36]
 / F_3CCl_3	A_{1-12}	-6.68	-6.68	-4.73	0	0	0	[36]
 / ZSM-5	A_1, A_4, A_5, A_8 A_2^*, A_3^*, A_6, A_7	-24.1 -7.3	-7.9 0.3	-17.4 -6.7	0 107.3*/72.7	0 0	0 0	[3]
 / CFCl_3	A_1, A_4, A_5, A_8 A_2, A_6, A_3, A_7	-23.0 -6.4	-23.0 -6.4	-16.2 -2.8	0 0	0 0	0 0	[38]
 / CFCl_3	A_{para} A_{ortho}^*, A_{ortho} A_{meta}	-26.9 -12.2 -	-7.9 -4.4 -	-18.3 -10.0 -	0 67.8*/112.2	0 180	0 0	[2]
 / Houdry-M46 silica-alumina	A_α A_β A_γ	-5.2 0.9 -4.7	-9.7 2.3 -12.2	-12.6 4.8 -16.7	0 0 0	0 0 0	0 0 0	[6]

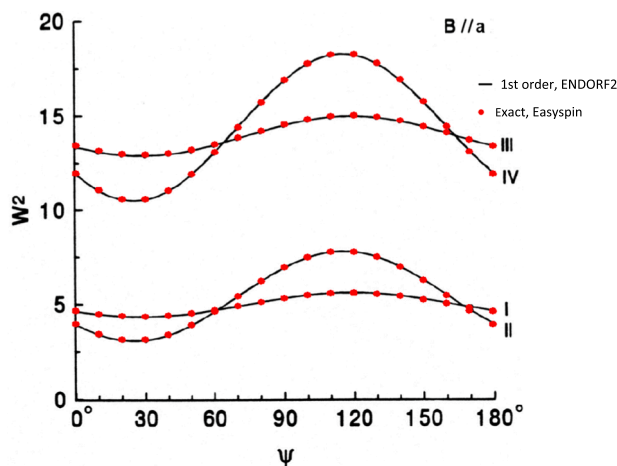


Fig. 1. Comparison of the square of the transition moments W^2 (arbitrary units) computed with 1st order theory (solid line), Eq (6), and exact methods in Easyspin (• dotted line), of the ^{14}N transitions I-IV of the $\text{CH}_2\text{NHCOC}_6\text{H}_5$ radical as a function of the RF-field orientation in the bc crystal plane of hippuric acid. The static field was aligned along the crystallographic a -axis, the RF-field was at an angle ψ with the c axis in the bc plane. The spin Hamiltonian parameters in [8] were employed.

$$\frac{d}{d\nu} \chi(B, \nu) = \int_{\theta} \sin \theta \int_{\varphi} \sum_j \left[s(B - B_j) I_j^2 \left(\frac{d}{d\nu} \sum_k t(\nu - \nu_{jk}) \int_{\psi} W_{jk}^2 d\psi \right) \right] d\varphi d\theta \quad (8)$$

A function similar to Eq (8) was derived by Kreiter and Hüttermann [12], based on the principles of powder ENDOR lineshapes developed by

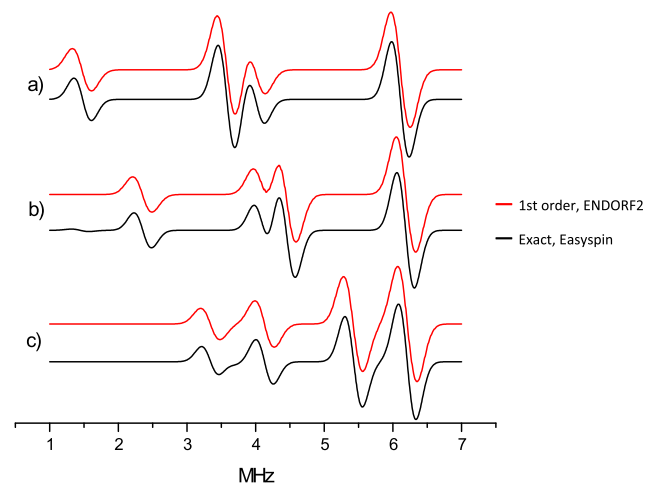


Fig. 2. Comparison of single crystal spectra of the $\text{CH}_2\text{NHCOC}_6\text{H}_5$ radical in hippuric acid simulated to 1st order with ENDORF2 (red, upper curves), and by exact matrix diagonalisation with EasySpin (black, lower curves) with the (1) static and (2) RF fields along the principal directions corresponding a) to the (1) -7.58 and (2) -9.44 MHz ^{14}N principal values, b) to the (1) -8.47 and (2) -7.58 MHz values, c) to the (1) -9.44 and (2) -8.47 MHz values, respectively, in Ref. [8]. Only the region containing ^{14}N -signals is shown.

Hoffman and coworkers [7]. The summations run over the EPR transition fields $B_j(\theta, \varphi)$ and the ENDOR transition frequencies, $\nu_{jk}(\theta, \varphi)$, connected to EPR transition j , with the corresponding transition probabilities $I_j^2(\theta, \varphi)$ and $W_{jk}^2(\theta, \varphi, \psi)$. The signal is integrated over all angles (θ, φ) of the static field \mathbf{B} in the molecular frame, and the ENDOR transition probability $W_{jk}^2(\theta, \varphi, \psi)$ is in addition integrated over angle ψ ,

the angle relating the molecular frame to the RF-field \mathbf{B}_2 , for each direction of the static field \mathbf{B} . The transition probability W_{jk}^2 is in general anisotropic and depends on the orientation of the species relative to both the static and the RF field [23,28]. In a powder all molecules with the same orientation with respect to \mathbf{B} will have the same resonance frequency, but they will be randomly oriented relative to \mathbf{B}_2 . Analytical integration of W_{jk}^2 over the distribution of \mathbf{B}_2 directions in the plane perpendicular to \mathbf{B} gives the expression (9) which is valid when \mathbf{B}_2 is in the plane orthogonal to \mathbf{B} . Analytical integration avoids the need for a time-consuming numerical integration of W^2 over Ψ .

$$W_{jk}^2 = \int W_{jk}(\theta, \varphi, \psi)^2 d\psi = \frac{1}{2} \left(\frac{B_2}{B} \right)^2 (\alpha C^2 \alpha - \alpha^* C \ell \bullet \alpha C \ell) \quad (9)$$

Here α is a vector with the components $\langle h | I_x | k \rangle$, $\langle h | I_y | k \rangle$ and $\langle h | I_z | k \rangle$, and α^* is obtained by complex conjugation of the components, C the ENDOR tensor in Eq. (7) and ℓ the unit vector specifying the static field direction. The nuclear index i has been dropped for simplicity. The integration is employed in a similar way as Kottis and Lefebvre [32] used for triplet state EPR spectra. The convolution function t is the line shape of the ENDOR transition. The component EPR line shape function s acts as a weighting function and selects the transitions that contribute to the ENDOR signal at a particular field setting. In the program Easyspin [15–17] the angular selectivity is instead set in the frequency domain by an excitation window around the microwave frequency. The angular selectivity depends on the ratio between the electron spin–lattice relaxation rate (T_{1e}^{-1}) and the electron spin–spin relaxation rate (T_{2e}^{-1}) [4]. Angular selectivity is efficient if $T_{1e}^{-1} \gg T_{2e}^{-1}$ which is the common situation for transition metal complexes and radicals in frozen solution above 77 K [29]. The ENDOR spectrum is then the sum of all transitions that are connected to the EPR transitions in resonance. In the other limit, when $T_{2e}^{-1} \gg T_{1e}^{-1}$, the ENDOR spectrum is the sum of all possible orientations irrespective of which part of the EPR spectrum that is monitored. This situation has been encountered for organic radicals at very low temperatures, <4 K [4,29]. This case is not dealt with in Eq. (8) but has been treated for $I = 1/2$ nuclei [4].

3. Applications in radiation research, surface- and bio-physics

Previous assignments of the radical structures obtained by ENDOR measurements on powder samples exposed to radiation or activated by other means were examined in this work by comparison with simulations based on exact theory [15–16]. Unless otherwise stated matrix diagonalisation was employed using the ‘matrix’ option in simulations with EasySpin [17].

3.1. Aromatic radicals with *hfc* due to ring protons and methyl substituents ($I = 1/2$)

Simulations were performed in early works to interpret the ENDOR spectra of aromatic radicals trapped on metal oxide surfaces [5,6] and more recently in zeolites and polycrystalline halocarbon matrices [2,3,33]. The *g*-factors were close to the free electron value and nearly isotropic. The assignments obtained using perturbation theory [2,3,5,6,36] were reexamined in this work by exact simulations. The orientation of the *hfc* tensors in Table 2 are specified by the Euler angles of the principal axes in an orthogonal coordinate system with the *z* axis perpendicular to the aromatic ring and with suitably chosen in-plane *x* and *y* axes. The orientation was not reported for the perylene cation in the seminal work by Clarkson et al. [5,6].

The isotropic coupling at positions 1 and 4 of the Jahn-Teller distorted benzene cation, $a_{\text{iso}} = -25.31$ MHz, is in satisfactory agreement with the previously reported value considering the differences in experimental conditions [33]. The principal values at positions 1 and 4 in Table 2 are close to $a_{\text{iso}} \times (0.5, 1.5, 1.0)$ as expected for an α -H coupling with the smallest *magnitude* along the C–H bond and with the

intermediate value perpendicular to the molecular plane [34]. The principal value of -26.0 MHz is therefore thought to occur perpendicular to the benzene ring, the value -11.1 MHz along the C–H bond. The principal values of -7.9 and -17.4 MHz at positions 1, 4, 5 and 8 of the naphthalene cation radical in the ZSM-5 matrix are for the same reason attributed to the components along the C–H bond and perpendicular to the molecular plane, respectively. One may further assume that the *hfc* tensors at the *para* positions of the biphenyl ion and at the γ positions of the perylene cation radical on Houdry-M46 silica-alumina are similarly oriented with the numerically smallest coupling along the C–H bond, the intermediate value perpendicular to the molecular plane. The principal values of the *hfc*-tensors at the positions 2, 3, 5 and 6 of the Jahn-Teller distorted benzene radical ion show approximate axial symmetry, however, which also applies for the naphthalene cation in the ZSM-5 matrix at the positions 2, 3, 6 and 7 and the biphenyl cation at the ortho positions. The orientation of these tensors could not be predicted from the ENDOR data and was estimated by simulation of the EPR spectra and by quantum chemistry calculations [35,36].

The Jahn-Teller distorted benzene ion: The EPR study by Iwasaki et al. [33] provided the first experimental evidence for a static distortion of the benzene cation yielding the $^2B_{2g}$ state, with major spin densities on the C1 and C4 atoms in low temperature matrices. The in-plane principal values of the tensor at the positions 1 and 4 in Table 2 of the $C_6H_6^+$ and $C_6H_5D^+$ ion radicals are in good agreement with the previously reported values, -10.4 and -37.2 MHz, while the value -21.3 MHz perpendicular to the molecular plane differs somewhat from that in Table 2. The *hfc* tensors at the equivalent positions 2, 3, 5 and 6 in Table 2 show approximate axial symmetry in agreement with previous results [33].

The ENDOR spectrum in Fig. 3 (a) was obtained at 30 K from an X-irradiated sample of $CFCl_3$ containing a small amount of C_6H_5D . The spectra of the two spin-density isomers in Fig. 3(b) and (c) were previously simulated with ENDORF2 [36].

The ‘matrix’ option in EasySpin [17] was employed for the simulation (d) using *hfc* tensors as in (c). The A^+ , B^+ , and C^+ lines were attributed to the high frequency transitions corresponding to the principal tensor components of the H1 and H4 nuclei. D^+ and D^- were assigned to the perpendicular components at the high and low frequency branches of the H2, H3, and H5 nuclei. The E^+ lines were partly attributed to *hfc* due to the deuterium nucleus. The principal values at the high and low spin density positions in Table 2 are in good agreement with the reported data for the $C_6H_6^+$ ion [33]. It was difficult to distinguish between the two conformations (b) and (c) by the ENDOR spectra because of the small spectral differences. The EPR results in Ref. [36] indicated that a structure with deuterium attached to a carbon atom with high spin density was slightly favoured over the structures with deuterium at the atoms with low spin density. A ratio of 0.62:0.38 was estimated from a least-squares analysis [36].

Methyl-substituted benzene cations: The *hfc* tensors determined in measurements on the toluene and *p*-xylene cations gave support for the stabilization of the $^2B_{2g}$ type of state [36]. The *hfc* tensor of the methyl protons was axially symmetric with $A_{\perp} = 56.34$ MHz, $A_{\parallel} = 58.38$ MHz for the toluene cation in the F_3CCl_3 matrix at a temperature of 120 K. The $^2B_{1g}$ ground state was observed for the *o*-xylene and *m*-xylene cations, however, due to the lifting of the orbital degeneracy of the e_{1g} orbital like for the benzene cation in a solid argon matrix [37]. The predicted geometries, isotropic 1H *hfc* and π -electron spin densities obtained by DFT (density functional theory) calculations supported the experimental results.

The dimeric benzene cation: $(C_6H_6)_2^+$ formed by X-irradiation of frozen solutions of benzene in $CFCl_3$ and CF_3CCl_3 was characterised with ENDOR and assigned to a π -electron complex as indicated in Table 2. The isotropic *hfc* constant, -6.03 MHz, obtained from the data in Table 2 agrees with the value reported in an early note [39]. The distance *d* in Table 2 between the benzene rings were estimated from the values of the anisotropic *hfc* coupling to be in the range 0.2–3 nm by a treatment similar to that applied to obtain the distance between the monomer units

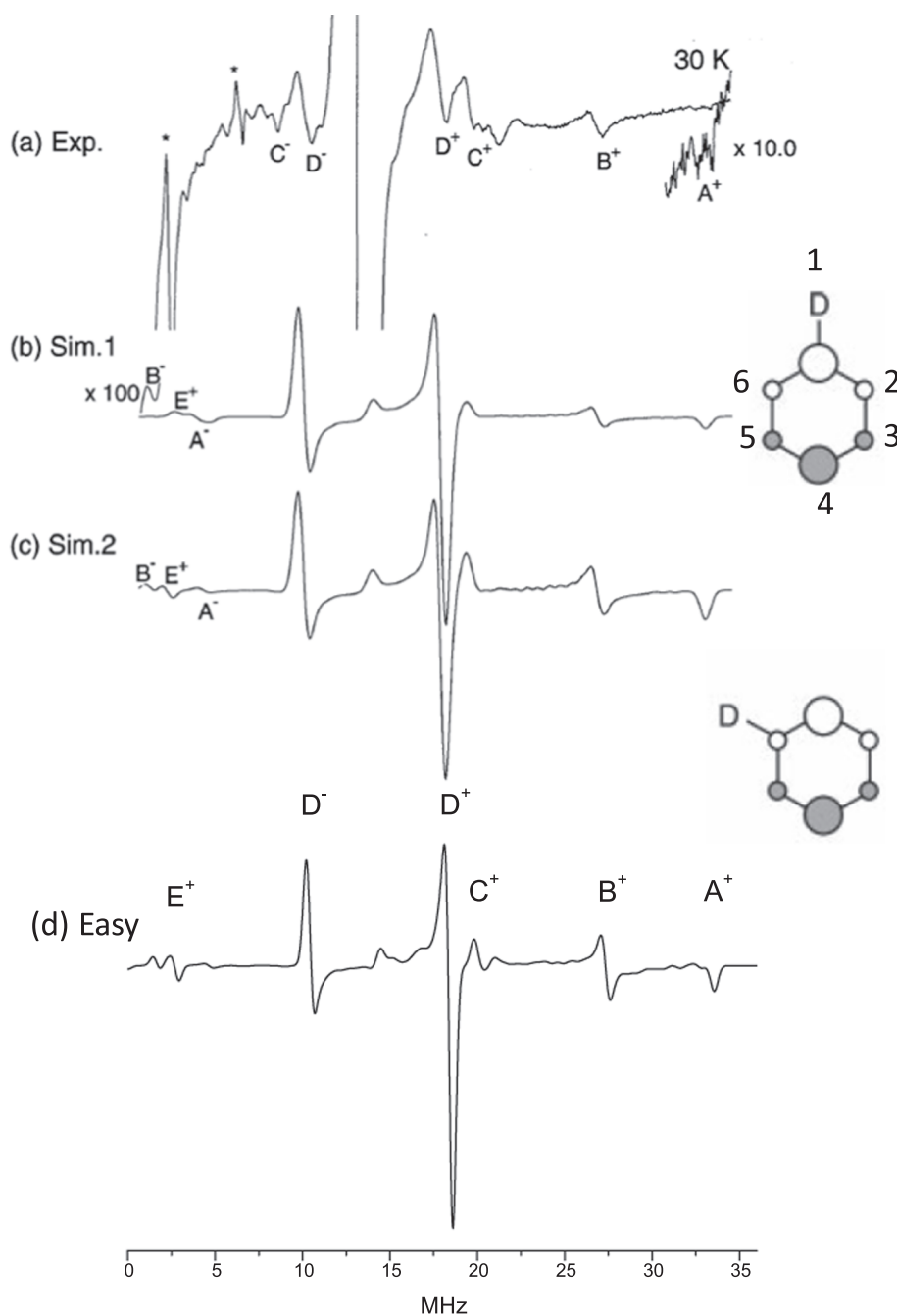


Fig. 3. (a) ENDOR spectrum at 30 K of an X-irradiated sample of CFCl_3 containing a small amount of $\text{C}_6\text{H}_5\text{D}$, obtained at the central transition of the EPR spectrum. (b) and (c) Simulated spectra using ENDORF2 of the two isomers of the $\text{C}_6\text{H}_5\text{D}^+$ radical cation with ^1H hfc principal values in Table 2, see also Table 1 of Ref. [36]. (d) Simulation of the 2nd isomer with hfc parameters as in (c) using the 'matrix' option in EasySpin [17]. Fig. 3a-3c were adapted from Ref. [36] with kind permission from the PCCP Owner Societies.

of fluorinated benzene cations in solid matrices [40]. Similar species have also been observed after the adsorption of benzene vapour on oxide catalysts [41].

The naphthalene cation radical: Two powder ENDOR studies of the naphthalene cation ($\text{N-H}8^+$) have been reported. In the first, $\text{N-H}8^+$ was produced by γ -irradiation of naphthalene in a CFCl_3 matrix. The obtained hfc tensors showed approximate axial symmetry at 140 K, presumably caused by a fast rotation about an axis perpendicular to the molecular plane [38]. In a second study $\text{N-H}8^+$ was produced by X- or UV-irradiation of naphthalene in H-ZSM-5 zeolite at 77 K [3]. The spectrum recorded at 116 K was interpreted by assuming a rigid structure. The ENDOR line positions obtained in the two studies coincided reasonably well, although the relative intensities were different. The reported hfc tensors of the (1, 4, 5, 8) and (2, 3, 5, 7) proton groups of $\text{N-H}8^+$ in the CFCl_3 and H-ZSM-5 matrices in Table 2 differed considerably, however, due to the different assignments of the observed transitions as

schematically indicated in Fig. 4. The $A_{\perp}(1)$ and $A_{\parallel}(1)$ lines in Fig. 4d were attributed to the high frequency transitions corresponding to the perpendicular and parallel principal directions of the (1, 4, 5, 8) group of protons of $\text{N-H}8^+$ in the CFCl_3 matrix [38]. The high and low frequency lines denoted $A_{\perp}(2)$ were attributed to the (2, 3, 5, 7) group of protons. The asymmetric line shapes denoted by asterisks in Fig. 4d were not apparent in the experimental spectrum [38] but might represent the parallel features of the (2, 3, 5, 7) group of protons. The assignment was supported by simulations of the EPR spectra obtained from γ -irradiated samples containing protonated or partly deuterated naphthalene in a CFCl_3 matrix [38]. Simulations of the ENDOR spectra were not presented, however.

The A_x^+ , A_y^+ and A_z^+ lines in Fig. 4c were attributed to the high frequency transitions corresponding to the x, y and z principal directions of the (1, 4, 5, 8) group of protons; A_y^- is the low frequency line corresponding to the y direction. The shape of the A_x^+ and A_z^+ lines of the exact

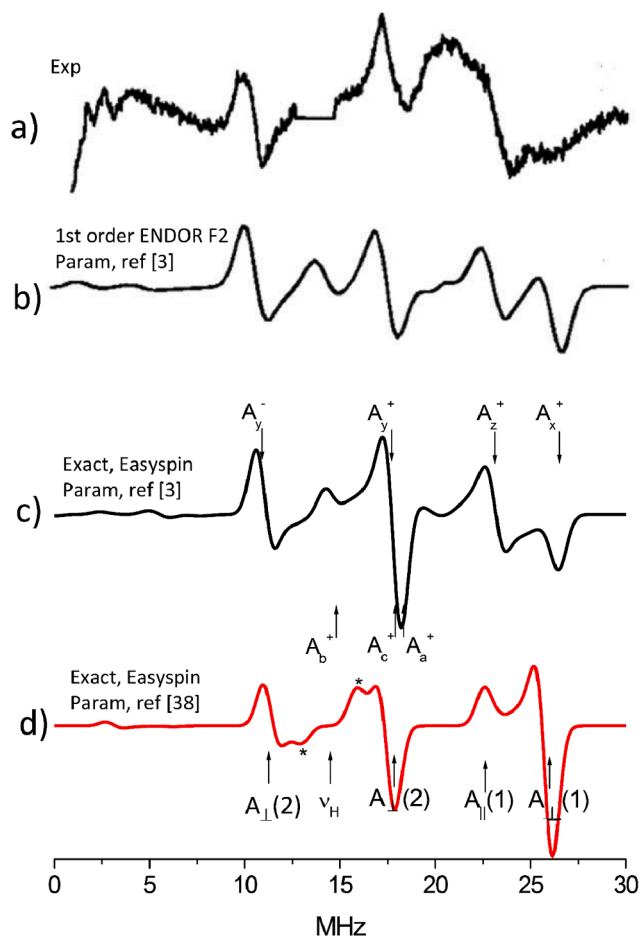


Fig. 4. (a) Experimental powder ENDOR spectrum at 116 K of the naphthalene cation radical in H-ZSM-5 zeolite obtained at the centre of the EPR spectrum ($B_{\text{obs}} = 341.69$ mT, $\nu = 9.57567$ GHz) [3,9]. The region of the intense matrix line at 14.55 MHz has been excluded. (b-d) Simulated spectra, (b) by 1st order theory with ENDORF2 using parameters from Ref. [3], (c) and (d) exact theory with EasySpin, (c) with hfc parameters from Ref. [3], (d) with axially symmetric hfc tensors from Ref. [38]. Fig. 4(a) and (b) were adapted from Fig. 6.5 in Ref. [9].

simulation (c) was found to agree more closely with experiment than was achieved with the previous first order ENDORF2 simulation in (b), adapted from Ref [9]. The high and low frequency lines due to the (2,3,5,7) group of lines denoted A_a^+ , A_b^+ , A_c^+ overlapped with those assigned to the (1,4,5,8) group. The relative intensities of the lines in (c) changed marginally by using the default orientation of the tensor axes available in EasySpin. Additional EPR and ESEEM measurements and spectrum simulations were reported in Ref. [3]. The two assignments in Fig. 4(c) and (d) are further considered in section 4.

The biphenyl cation radical, Ph_2^+ : The experimental and simulated ENDOR spectra of Ph_2^+ in CFCl_3 shown in Fig. 5 were obtained at the centre of the EPR spectrum.

The assigned lines are caused by intensity build-up at positions corresponding to the principal values of the anisotropic *para* and *ortho* proton hfc tensors. The lines are placed symmetrically around the proton Larmor frequency ν_H at 14.54 MHz. Fluorine matrix nuclei and *meta* protons with small hfc constants were excluded in the simulations. They produce lines in the region 10.5 to 16.5 MHz in the experimental spectrum [2]. Intensities were calculated to first order including enhancement, but neglecting relaxation and instrumental effects in the simulation shown in Fig. 5(b). The relative intensity distribution was predicted, but slightly overestimated in comparison with the experimental spectrum. As can be seen from Fig. 5(b) and (c) the lines below ν_H

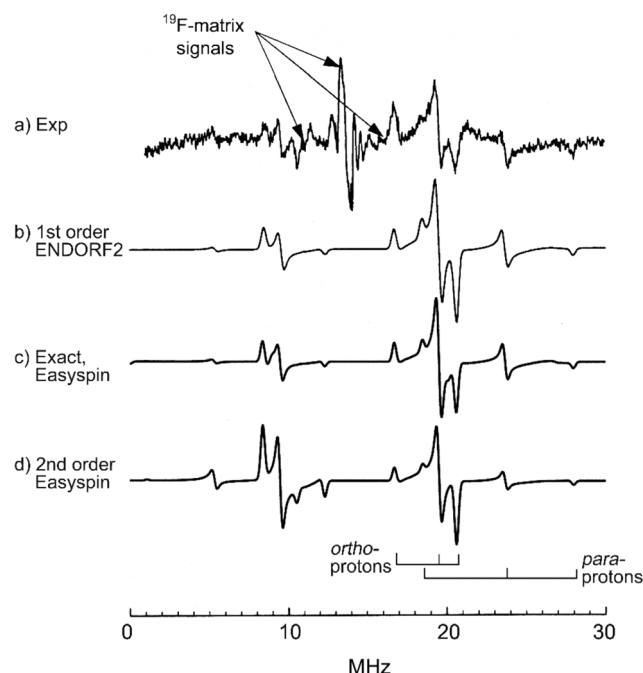


Fig. 5. Experimental (a), simulated to 1st order (b), exact (c), and second order (d) powder ENDOR spectra of the biphenyl radical cation in CFCl_3 matrix at 120 K. The simulated spectra were calculated using the spin Hamiltonian parameters from Ref. [2], at magnetic field $B = 341.40$ mT and microwave frequency $\nu = 9.5670$ GHz. The simulations included *para*- and *ortho*-protons (spectral lines above ^1H -Larmor frequency indicated), but matrix fluorine and *meta* protons were excluded. The weight function s and convolution function t , see Eq. (8), had line widths of 0.1 mT and 0.3 MHz (both Gaussian shaped) in (b). The simulations in (c) and (d) employed an excitation width of 2.8 MHz, and an ENDOR line width of 0.35 MHz. Figures (a) and (b) were adapted from [2] with kind permission from Elsevier.

are of lower intensity than the matching lines above, which we attribute to the hyperfine enhancement effect. The simulations (c) and (d) were both made using EasySpin [17] with theoretically obtained orientations of the *ortho* and *para* hfc tensors axes, case (c) with exact calculation including hyperfine enhancement, and case (d) using the 2nd order perturbation theory of Iwasaki [24]. The relative intensities of the lines in (c) changed significantly by using the default orientation of the tensor axes available in EasySpin.

The perylene cation radical: Radicals of aromatic radicals formed on activated metal oxide surfaces have been investigated by EPR methods for more than 50 years. Simulations of ENDOR spectra were first reported by Clarkson et al [5,6]. The contributions from each of the three inequivalent groups of protons at the α , β , and γ positions of the perylene cation radical were calculated separately and added. The simulated and experimental spectra were superimposed to show the degree of agreement [6]. The spectrum of all twelve protons could not be calculated with the 'matrix' option in EasySpin due to memory overflow. The spectrum obtained using the 'perturb2' option, shown in Fig. 6 was, however, in satisfactory agreement with the experimental and simulated spectra in the original works [5,6]. The contributions of each group of protons are labeled with +/- signs for the high/low frequency lines and the symbols x, y, z for the principal values.

3.2. Alkyl radicals with hfc due to α and β protons ($I = 1/2$)

Irradiated samples of saturated organic compounds frequently contain radicals with relatively large anisotropic hfc constants of the α - and β -protons attached to the carbon radical centre and to adjacent carbons, respectively. Three radicals were identified by EPR and ENDOR measurements in single crystals and powders of X-irradiated L-alanine.

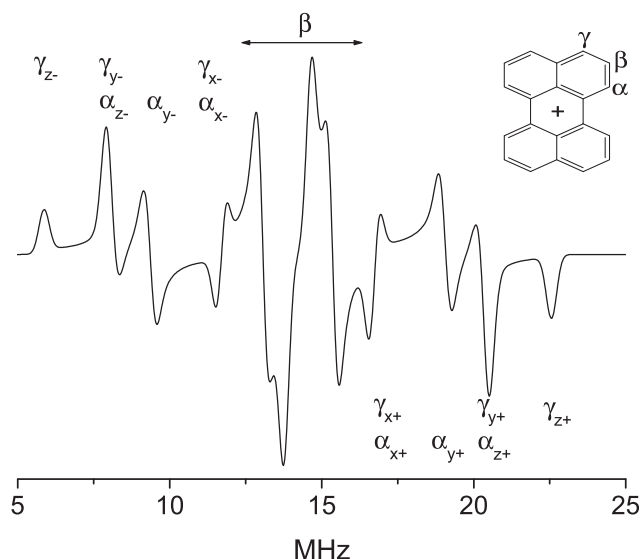


Fig. 6. Simulated ENDOR spectrum of the perylene cation radical on Houdry-M46 silica-alumina [6] with the 2nd order option in EasySpin [17], employing an ENDOR line width of 0.4 MHz (Gaussian) and g - and hfc -tensor parameters in [6]. Contributions due to the α -, β - and γ -protons, with subscripts x, y, z for the principal values and $+/+$ for the $m_s = \pm 1/2$ lines are indicated.

The ENDOR powder signals attributed to $\text{CH}_3\dot{\text{C}}\text{H}_4\text{COOH}$ (R1) and $\text{H}_3\text{N}^+\dot{\text{C}}(\text{CH}_3)\text{COO}^-$ (R2) could be measured separately by saturating the central and the outermost high-field EPR resonance line, respectively [42,43]. The prominent features in Fig. 7 a) are due to the methyl protons in the β position of R1, having nearly axial hfc splittings, with perpendicular and parallel features marked with long and short bars and label H_3C .

3.3. Radicals with hfc and nqc splittings due to nuclei with $I \geq 1$

Simulations with Easyspin were performed to validate the interpretations obtained with 1st order software of spectra with modest and large nqc due to ^{14}N .

^{14}NO -ligated ferrocycytochrome c -heme $a3$: The powder ENDOR spectra obtained by LoBrutto et al [44] were previously simulated employing exact diagonalization of the spin Hamiltonian, but with transition probabilities to zeroth order [12]. Nitrogen ENDOR signals were detected from the histidine and NO ligands of the central ferrous ion.

The spectra (absorption line shape) in Fig. 8 were all calculated with the parameters in Refs. [12,44] to show the degree of agreement obtained by the three different methods. The nqc constants are small compared to the hfc . All tensors have parallel principal directions except the A-tensor of the NO-nitrogen which is rotated 17.5° around the x -direction. The spectra were obtained at $g = 2.079$, near the principal value $g = 2.082$. The peak positions obtained with ENDORF2 using first order perturbation theory in Fig. 8 a) agree well with those calculated with Easyspin using exact diagonalisation, Fig. 8 b), and second order perturbation theory, Fig. 8 c), except for the peak with highest intensity, near 15.8 MHz, which is shifted to higher frequency by around 0.15 MHz in (a). Line positions of Fig. 8 a) agreed within less than 0.07 MHz with results obtained in a previous simulation employing exact diagonalisation, and agreement with experimental peak positions was as good as in [12]. The transition probabilities in Fig. 8 a) were calculated by Eq.(9), which is valid to first order since the g -anisotropy fulfills the condition $(1/g^2) \times \text{rgg} \ll 1$. Excitation widths up to 150 MHz have been successfully tested for this case. The relative intensities of the histidine and NO-nitrogen lines are similar in Fig. 8 a) and b), but are quite different from c), as well as the simulation in Ref. [12], where transition probabilities were calculated to zeroth order. The intensity distribution in

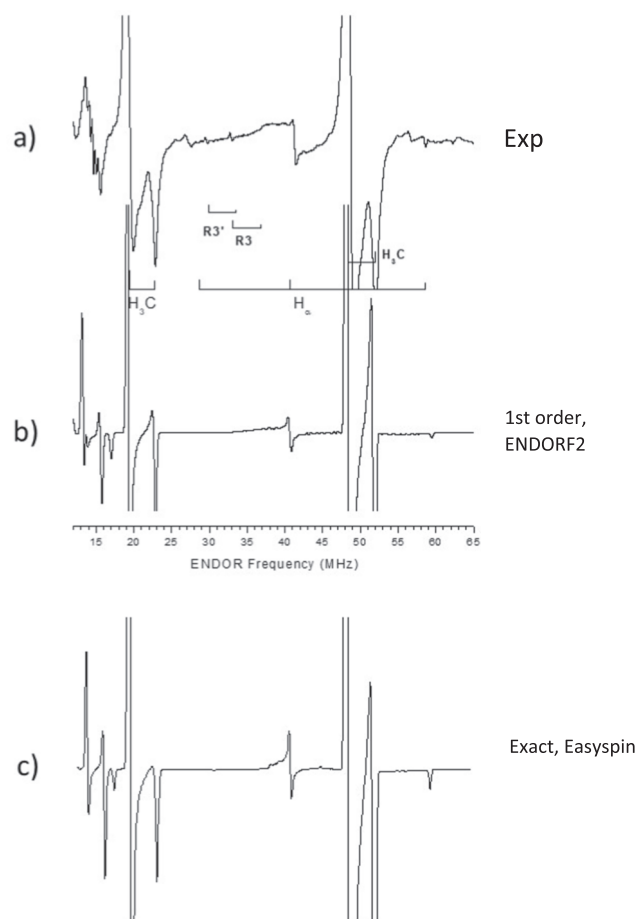


Fig. 7. a): First-derivative X-band powder ENDOR spectrum of the $\text{CH}_3\dot{\text{C}}\text{H}_4\text{COOH}$ (R1) radical featuring resonances due to H_α and CH_3 marked in the figure and lines attributed to weakly coupled protons in the low frequency wing. The spectrum was obtained at 221 K by saturating the central EPR line of an X-irradiated polycrystalline L-alanine sample. b) and c): Simulated ENDOR spectra using (b) ENDORF2 employing weight function $s = 0.3$ mT and convolution width $t = 1.0$ MHz (both Gaussian); (c) Easyspin using the 'matrix' option, 0.3 MHz line width (Gaussian), and default (infinite) excitation width. Spin Hamiltonian parameters given in [43] were employed. Fig. 7(a) and (b) were adapted from spectra provided by Prof. E. Sagstuen.

Fig. 8 a) and b) does not perfectly reproduce the experiment in Ref. [44], but the agreement with experiment is substantially better than simulations obtained in either c) or using the zeroth order intensities in [12].

The $\dot{\text{C}}\text{H}_2\text{NHCOC}_6\text{H}_5$ radical: The capability of the theory developed in [8,9] to analyse the powder ENDOR spectra of a species with an appreciable nqc interaction was investigated for the $\dot{\text{C}}\text{H}_2\text{NHCOC}_6\text{H}_5$ radical fragment in X-irradiated polycrystalline hippuric acid [45]. Only the region containing ^{14}N -signals is shown in Fig. 9. The lowest ENDOR lines could not be experimentally observed as the region below 2 MHz is affected by a sharp decline in baseline and other instrumental effects. The experimental spectrum was obtained at 110 K in the centre of the EPR spectrum. The g -anisotropy is small and was neglected. The nitrogen nucleus is characterized by a substantial nqc term compared to the hfc and nuclear Zeeman splittings. The microwave frequency, field setting, and α - ^1H and ^{14}N -parameters in [8] were used in the simulations, including the nqc terms in Fig. 9 b), d), and e), but excluding them in Fig. 9 c). The nitrogen parameters $A(^{14}\text{N}) = (-7.58-8.47-9.44)$ and $Q(^{14}\text{N}) = (-0.843\ 0.582\ 0.261)$ MHz, are those of Ref. [45] apart from the two principal hfc values of smaller magnitudes, which were slightly altered [8] to improve the fit.

The hfc tensors of the two α -protons included in the calculation were as in Ref. [45]. Simulations b) and c) employed a Gaussian weight

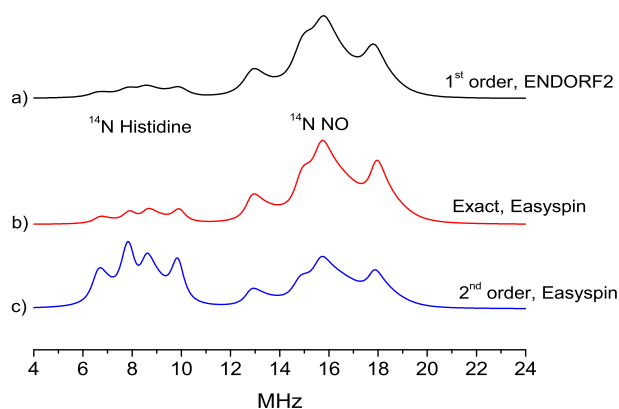


Fig. 8. Simulated powder ENDOR spectra (in absorption) of ^{14}N -ligated ferrocyanide c heme a3, at the field setting ($g = 2.079$) in the X-band EPR spectrum ($\nu = 9.32$ GHz). The simulation in a) employed a line width of 0.6 mT in weight function s (Gaussian shape) and a line width of 0.5 MHz in the ENDOR convolution function t (Lorentzian shape) of Eq. (8). The simulations in (b) and (c) employed an excitation width of 16.8 MHz, and an ENDOR line width of 0.6 MHz (Lorentzian shape). Fig. 8(a) was adapted from [8] with kind permission by Elsevier (1996).

function s (see Eq. (8)) with line width 0.1 mT and Lorentzian convolution function t with line width 0.5 MHz. Simulations d) and e) used the 'matrix' option in Easyspin with a line width of 0.35 MHz. A finite excitation width, of 2.8 MHz in d) gave a significantly better fit to the experimental curve in a) than the infinite excitation width in e). The simulation with the 2nd order option [17] (not shown) disagreed with the experimental spectrum, however. Similar hfc tensors were reported in a re-investigation of hippuric acid single crystals X-irradiated at 195 K [46].

3.4. hfc splittings in ENDOR spectra due to matrix- and ligand nuclei

The hfc splittings of matrix nuclei can provide information about the trapping sites of radicals in a solid matrix [1,42,43,47–49]. Single crystal measurements are preferable, but not always available. Some data can however be deduced even from the powder spectrum.

The $\dot{\text{C}}\text{O}_2\bullet\bullet\text{Li}^+$ radical: Radiation-induced $\dot{\text{C}}\text{O}_2$ radicals were found to interact with several ^7Li -nuclei and protons in ENDOR studies of X-irradiated crystal and polycrystalline samples of lithium formate monohydrate ($\text{LiHCO}_2\cdot\text{H}_2\text{O}$). Splittings due to ^7Li nqc interactions were not observed. Simulations of the powder spectra were reported to be in reasonable agreement with experiment [48,49]. Additional simulations using different options with the EasySpin software were performed in this work to validate the results obtained with other software, Fig. 10. The contributions of the matrix protons [49] had to be excluded to avoid memory overflow in the simulations (c) and (d), which were made using exact theory [17]. The close agreement between the spectra is noteworthy, considering that the different orientations of the ^7Li hfc tensor axes [49] were accounted for in (d), but were neglected in (c). The agreement of spectrum e) with (c) and (d) indicates that the 2nd order perturbation theory by Iwasaki [24] is adequate for this system. A calculation with this method including the ^7Li and ^1H ENDOR lines was completed within a few seconds. The line shape at 5.6 MHz of the simulated spectra deviates somewhat from the experimental line in Fig. 10 b), possibly due to a slight uncertainty of the ^7Li tensors.

Angular selection: In cases when the EPR spectrum is dominated by a single anisotropic coupling it is sometimes possible to resolve portions that correspond to a single orientation. Rist and Hyde were the first to use the dominating g -anisotropy of Cu and Ag complexes to obtain single crystal-like ENDOR spectra at g -value extrema in the powder EPR spectrum [50]. The ability to simulate angular selection effects was

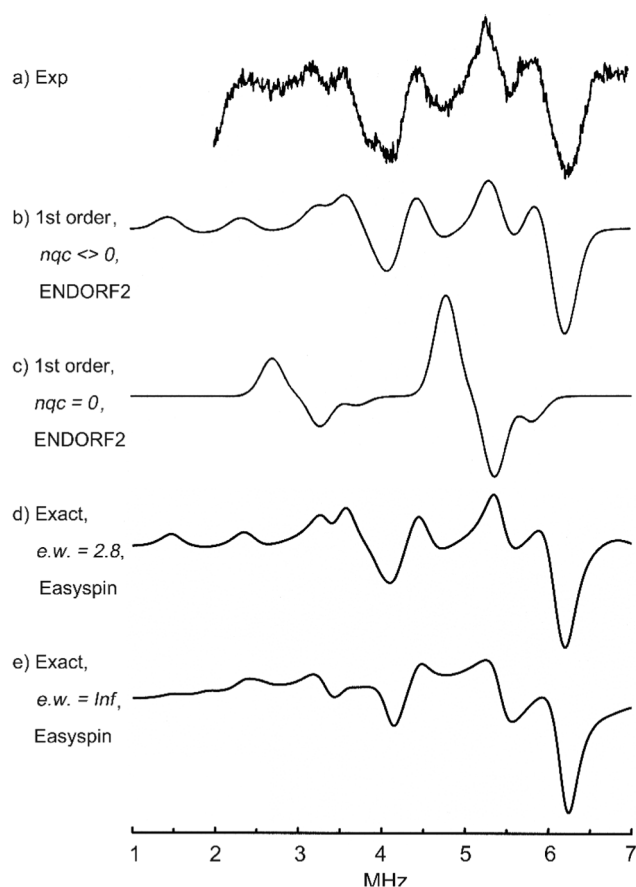


Fig. 9. Experimental a) and simulated b) – e) ENDOR spectra at 110 K of the $\dot{\text{C}}\text{H}_2\text{NHCOC}_6\text{H}_5$ radical fragment formed in X-irradiated polycrystalline hippuric acid. Only the region containing ^{14}N -signals is shown. The ^{14}N parameters in [8] were used in simulations, b), d), and e) including, but c) excluding nuclear quadrupole terms. The hfc tensors of the two α - ^1H were as in Ref. [45]. Simulations in b) and c) employed a Gaussian line width of 0.1 mT in weight function s of Eq. (8), and an equivalent excitation width (e.w) in d) of 2.8 MHz. The simulation in e) employed an infinite excitation width. Simulations in b) and c) employed a Lorentzian convolution function t with line width 0.5 MHz, and in d) and e) an ENDOR line width of 0.35 MHz. Fig. 9 a)–c) were adapted from [8] with kind permission from Elsevier (1996).

examined in this work by comparison of the simulations with the exact method in [17] and by the theory in [8,9]. Reasonable agreement was obtained for the hfc features due to the ligand nuclei of Cu(II)-ZSM complexes [51–53], indicating that the method developed in [8,9] was applicable also for the simulation of $S = 1/2$ metal ion complexes with appreciable g -anisotropy. Angular selection was not observed in the X-band spectra of organic radicals, as there is usually no single dominating coupling to obtain such 'single crystal' spectra, which instead are made up of a large number of orientations. The lack of a dominant g -anisotropy for this type of radicals can actually be an advantage in some cases. An example is when the EPR spectrum consists of an odd number of lines and the g -anisotropy is small. In the centre of the powder spectrum contributions from all orientations overlap. An ENDOR spectrum obtained at this position will contain contributions from practically all directions. In this case it may be possible to observe all the principal components of a hfc tensor in the same spectrum, as demonstrated e.g. in simulations of the experimental spectra due to the biphenyl and naphthalene radical cations [2,3,8,9].

4. Discussion

Several software packages have been developed to obtain the hfc and

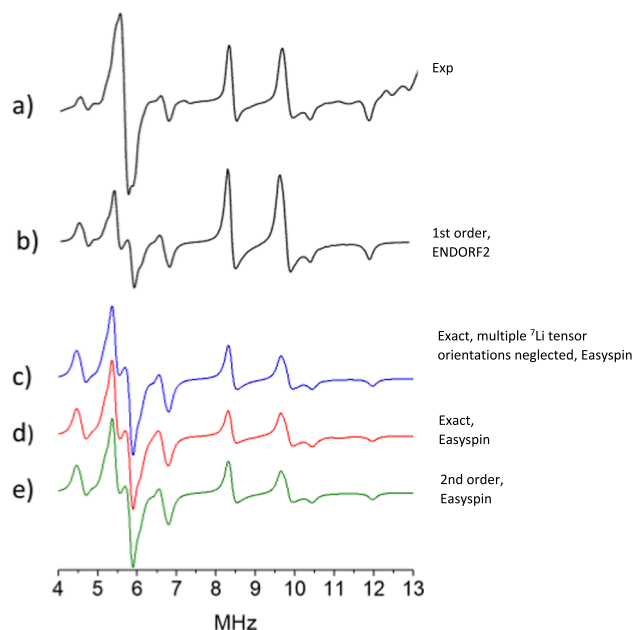


Fig. 10. Experimental a) and simulated b)–e) first derivative ENDOR spectra of polycrystalline $\text{HCO}_2\text{Li}\cdot\text{H}_2\text{O}$, irradiated by X-rays to a dose of 25 kGy at 295 K and measured at ca. 200 K. The contributions of the matrix protons [49] are excluded, and only the region containing ^7Li -signals is shown. The simulated spectra were calculated with the g- and ^7Li hfc-tensors in Ref. [49], employing ENDORF2 in b), EasySpin with exact theory in c) and d), 2nd order theory in e). The different orientations of the ^7Li hfc tensor axes [49] were accounted for in b), d) and e), but were neglected in c). Fig. 10 a) and b) were kindly provided by Prof. E. Sagstuen.

nqc tensors of free radicals by the simulation of powder ENDOR spectra [2–18]. Comparisons of the results obtained by 1st order and exact theory have not previously been extensively made, however. Experimental spectra of a few aromatic- and bio-radicals were analysed in early work [8,9] and compared with results obtained by simulation methods that were available at that time. Several ENDOR studies of powdered samples have since then been reported [36,38,43]. In the previous works by the present authors simulations based on the 1st order theory in [8] were employed to obtain the hfc tensor, along with the nqc tensor for nuclei with $I \geq 1$.

A comparative analysis of powder ENDOR spectra simulated by exact and 1st order theory was performed in this work for several free radical systems of interest in radiation research, surface and quantum chemistry, biochemistry and related fields. The values of the anisotropic hfc and nqc tensors were extracted by simulations with the EasySpin software [15–17]. By using the 1st order treatment in [8] errors of the order 0.01 MHz were estimated for ENDOR frequencies up to ca 20 MHz [55, pp193–194]. These errors can be neglected for the aromatic radicals, and also for the determination of the hfc and nqc tensors due to ^{14}N in bio-radicals [8] and to the hfc tensors of matrix ions and ligand groups considered in Section 3. This indicates that the principal values of the tensors can be extracted in these cases by fitting to the experimental ENDOR spectra even by 1st order theory. Larger errors, of the order 0.2 MHz, were estimated for the strong ^1H hfc of aliphatic radicals [28]. A simple 2nd order equation is available to improve the fit [24] but was not implemented in the present work.

One might have expected that the line shapes were affected by the orientation of the different tensors, thereby providing a means to estimate the relative orientations of the corresponding principal axes. The orientation of the tensors was difficult to obtain by this method, however. For the biphenyl cation the relative intensities of the lines in Fig. 5 were strongly affected by the relative orientation of the axes due to the ortho and para protons. For the naphthalene cation the influence was

marginal, however. The different results indicate that the analysis is complex. The orientations employed in the simulations were instead obtained from previous EPR single crystal studies [33,42,43,49], by quantum chemistry calculations [2,3,8], and from the known principal directions of the proton tensor in the α -position of an organic radical [34]. Some details of relevance for the specific systems are given below.

Large aromatic cation radicals trapped on surfaces: The program used in the early studies by Clarkson et al [5,6] might have been the earliest one for the simulation of powder ENDOR spectra of large systems with anisotropic hfc due to several protons but may no longer be available. Exact simulations with EasySpin are still time-consuming for such systems [17]. The simulation in Fig. 6 indicates, however, that the 2nd order perturbation treatment by Iwasaki [24] implemented in EasySpin, is of acceptable quality, even though the allowed transition moments are all set equal to one [17]. Better fitting might be obtained by implementing formulae like those in Ref. [8] for the transition moments in the 2nd order option of the EasySpin package. This development is outside the scope of the present work, however.

The benzene cation radical: Exact simulations [17] were employed to improve the agreement with the transition strengths observed experimentally [2–4,36], and to allow comparisons with the spectra earlier calculated to 1st order [8–10]. The ^1H hfc tensors of the C_6H_6^+ and $\text{C}_6\text{H}_5\text{D}^+$ ions at 30 K in Table 2 agree closely and are in reasonable agreement with the previously reported tensors obtained in EPR studies at 4 K [33]. The good agreement of the ENDOR spectra obtained in the simulations with EasySpin and ENDORF2 for the $\text{C}_6\text{H}_5\text{D}^+$ ion further supports the assignment. The influence of methyl substitution has been discussed elsewhere [36].

The naphthalene cation radical: The isotropic hfc constants of the naphthalene cation radical have so far been indirectly determined from the data of the symmetric dimer with the spin density distributed between the two units [57]. The hfc constants of the two equivalent groups of protons, obtained by EPR measurements on the dimer cation in liquid solution [57], correspond to $a_1 = -15.5$ MHz, $a_2 = -5.77$ MHz for the monomeric cation, in reasonable agreement with the values observed in the frozen boric glass [56] and on H-ZSM-5 zeolite [3]. The a_2 constant agrees with the value observed by ENDOR in polycrystalline CFCl_3 , considering the different experimental conditions, while there is a large difference between the coupling constant of the 1,4,5,8-protons, $a_1 = -20.74$ MHz, observed in Ref. [38] with those in other works [3,56,57].

The validity of the assignment in Ref. [3] was investigated by comparison of the experimental and calculated (within parentheses) dipolar hfc constants, -7.66 (-7.30), 8.59 (9.92), -0.94 (-2.63) MHz for the (1, 4, 5, 8) set of protons and -2.89 (-2.92), 4.97 (5.28), -2.06 (-2.37) MHz for the (2,3,6,7) set. The calculated hfc constants are seen to be in reasonable agreement with this assignment, in view of the approximate semiempirical method employed in [3] and of the experimental uncertainties in the determination of the tensor components. The approximate axial symmetry of the tensor due to the (H_2 , H_3 , H_6 , H_7) protons observed experimentally was also apparent in the theoretical data. The electronic structure of this species has been thoroughly investigated [58], but calculations of the hfc constants with accurate methods may not be available. A similar analysis of the tensor data obtained in Ref. [38] is complex due to the assumed rapid rotation of the ion in the CFCl_3 matrix and was not attempted. The simulation in Fig. 4d was, however, in rather poor agreement with the experimental ENDOR spectrum in Ref. [34] using the hfc tensors determined in that work.

The biphenyl cation radical: The isotropic hfc constants of the biphenyl cation obtained in this work, $a(\text{ortho}) = -8.9$ MHz, $a(\text{para}) = -17.7$ MHz, are in excellent agreement with the values in trifluoroacetic acid solution, $a(\text{ortho}) = -8.8$ MHz, $a(\text{para}) = -17.6$ MHz, in view of the different experimental conditions [59]. A small coupling, $a(\text{meta}) = 1.43$ MHz, observed in the liquid state was not resolved, however. The dipolar couplings, $\mathbf{B}(\text{ortho}) = [-3.3, 4.4, -1.1]$ MHz, $\mathbf{B}(\text{para}) = [-9.2, 9.8, -0.6]$ MHz, obtained by subtracting the isotropic coupling, are also of reasonable magnitudes, taking in account the π -electron spin densities,

$\rho(\text{ortho}) = 0.105$, $\rho(\text{para}) = 0.208$ at the carbon atoms [59]. By applying the relations $a = Q \cdot \rho$, $B_2 = K \cdot \rho$ for the isotropic and dipolar coupling constants of a proton attached to a carbon atom of a π -electron radical, one obtains B_2 values of 4.9 and 9.8 MHz along the C–H bond, using the empirical values of K and Q in Ref. [60] and appropriate spin densities ρ at the *ortho* and *para* positions. The agreement with the corresponding experimental value of 4.4 and 9.8 MHz might be fortuitous, considering that the dipolar coupling can be caused by the interaction with π -electron spin densities at more than one carbon atom. This possibility has been considered [49] but was not accounted for in the present work. To our knowledge more advanced computations are not available.

Alkyl radicals: The experimental and simulated features of the H_α -protons in alkyl radicals are weak in polycrystalline matrices because of the large *hfc* anisotropy, while the line-shape with modest anisotropy due to the methyl protons of the R1 radical, $\text{CH}_3\dot{\text{C}}\text{H}_\alpha\text{COOH}$, in X-irradiated L-alanine [43,44], was well resolved. The 2nd order effects discussed in [28], which were not implemented in the ENDORF2 software, might cause line shifts up to ca 0.2 MHz. The simulated powder spectra in Fig. 7 were, nevertheless, in satisfactory agreement with experiment.

Radicals with *hfc* and *nqc* splittings due to nuclei with $I \geq 1$. Provided that the electronic Zeeman term is dominant, the theory developed in [8,9] applies for nuclear spins $I \geq 1$, even for arbitrary relative magnitudes of the *hfc* and nuclear terms. This view was supported by the exact simulations in Fig. 8 of a ferro-cytochrome complex with relatively small *nqc* terms and in Fig. 9 of the $\dot{\text{C}}\text{H}_2\text{NHCOC}_6\text{H}_5$ radical fragment in polycrystalline hippuric acid with an appreciable *nqc* splitting in the ^{14}N ENDOR spectrum. In these cases the line-shape depended on the relative orientations of the *hfc* and *nqc* tensors of the ^{14}N nucleus. The strong dependence of the excitation width parameter in Fig. 9 was another noteworthy observation. A similar dependence was previously observed for the corresponding weight function employed in the ENDORF2 software [8].

***Hfc* splittings due to matrix- and ligand nuclei:** ENDOR measurements of the *hfc* splitting of weakly interacting matrix nuclei have allowed a detailed mapping of the solvation shell of the trapped radicals formed in early work [1,49]. The simulations obtained in the present work have indicated that the 2nd order perturbation option in EasySpin can be employed to obtain the principal values but not the spatial arrangements of four Li^+ ions about the CO_2^- radical in X-irradiated Li-formate powder.

5. Summary

The anisotropic *hfc* constants of ring protons and methyl groups in aromatic radicals were accurately determined by exact simulation of the experimental powder ENDOR spectra. The performance of software using perturbation theory [5,6,8,9] was examined.

The proton splitting constants of aliphatic radicals in α -position could not be determined due to the appreciable anisotropy, yielding weak signals. The ^1H tensor in β -position was accounted for by simulations, however.

Simulations were employed for the assignment of spectra due to nuclei with $I \geq 1$ taking in account the influence of the relative orientation of the *hfc* and *nqc* tensors on the line-shape.

ENDOR measurements of the *hfc* splittings by weakly interacting matrix nuclei were analysed.

ENDOR simulation programs known to us were presented in an Appendix.

6. Supporting information

The anisotropic *hfc* constants of aromatic and aliphatic radicals trapped in frozen solutions or on zeolite surfaces were previously determined by simulations using perturbation methods [2,3,5,6,8–10,36,49]. The *hfc* parameters were adjusted for best agreement with experimental spectra. The ENDORF2 software, the input

data files to run the program, an article describing the theory [8,9] and a manual were deposited as DOI <https://doi.org/10.5281/zenodo.4670928> at <https://github.com/EndorF2/Simulation>. ENDORF2 is a Fortran77 program for the simulation of ENDOR spectra of free radicals in single crystals and powders, treating the *hfc*, *nqc* and nuclear Zeeman interactions as a joint perturbation [8–10]. Diagonalisation of the perturbation Hamiltonian, H_i in Eq. (2), can be performed numerically for any nuclear spin in the range $\frac{1}{2} \leq I \leq 9/2$. An analytic treatment available for nuclei with $I = 1/2, 1$, and $3/2$ [54] is ca 30 % faster. Further information is available in Ref [8] available at <https://github.com/EndorF2/Simulation/>. The performance of the ENDORF2 program used in previous studies was examined by comparison with simulations using exact treatment employing input files deposited at github. Line-shapes like those in Fig. 5 for the biphenyl cation, Fig. 8 for the ^{14}NO -ligated ferrocycytochrome c, and Fig. 9 for the radical $\dot{\text{C}}\text{H}_2\text{NHCOC}_6\text{H}_5$ in X-irradiated polycrystalline hippuric can be obtained by running the ENDORF2 program with the provided input files. The ENDORF2 software, a manual, and an article treating the used theory [8,9] are available at the same site.

An exact treatment using EasySpin [15–17] was employed for the simulations in the present work. EasySpin is an open-source MATLAB toolbox for the simulation of a wide range of electron paramagnetic resonance (EPR) spectra [15–17]. It supplements the numerical and visualization power of MATLAB with the best computational methods devised by EPR spectroscopists. An arbitrary number of electron and nuclear spins can be treated. EasySpin is available free of charge. Matlab version 7.5 or later must, however, be installed on the computer and is not provided with EasySpin. Additional information is deposited at <https://www.easyspin.org/>. Matlab scripts for the simulation of the spectra due to monodeuterated benzene cation featuring Jahn-Teller distortion, the naphthalene and biphenyl cation, and of certain alkyl radicals with ^{14}N *hfc* and *nqc* interactions of comparable magnitudes [8,9] have been deposited at github. Simulation of alkyl radicals with large *hfc* due to ^1H is feasible using the appropriate script at the github site.

CRediT authorship contribution statement

Roland Erickson: Methodology, Software, Investigation. **Anders Lund:** Resources, Supervision, Validation.

Declaration of Competing Interest

The authors declare that they have no known competing financial interests or personal relationships that could have appeared to influence the work reported in this paper.

Appendix A. ENDOR simulation software

While EPR simulation software has been available for more than 50 years, procedures for the calculation of ENDOR spectra in solids were published considerably later, see e. g. [5,6,8–10] for early applications to disordered systems using perturbation treatments. Recently developed software, based on exact diagonalization of the spin Hamiltonian [11–18] and accounting for hyperfine enhancement and angular selection effects, have in many instances replaced previously used perturbation methods [2–10]. Relaxation effects have rarely been considered, however. The ‘hybrid’ method in [8,9] made it possible to compute first order ENDOR spectra of radicals containing nuclei with $I \geq 1$ having anisotropic *hfc* and *nqc* couplings of comparable magnitudes. Several of the listed programs in Table A1 are applicable both for EPR and ENDOR simulations and can handle complex spin systems. Exact numerical diagonalisation was employed in the present investigation using the EasySpin package to validate the performance of the ENDORF2 program used in previous works.

EasySpin: EasySpin is a Matlab toolbox for the simulation of EPR and

Table A1

Programs for the simulation of powder ENDOR spectra (accessed 2022–02-05).

Program	Order	Reference
EasySpin	Exact, 2nd order	https://www.easyspin.org/
EPR-NMR	Exact	[13], https://faculty.chem.queensu.ca/eprnmr/
XEMR	Exact	https://github.com/jmeloranta/xemr
XSOPHE-SOPHE	Exact	[14], https://www.bruker.com/products/mr/epr/epr-software/simulation-suites
Sim	Exact	Dr H. Weihe, Department of Chemistry, University of Copenhagen
MAGRES	Exact	[11]
MSPEN (EPR/ENDOR)	Exact	[12]
GENDOR ($S=\frac{1}{2}$)	1st order	[7], https://chemgroups.northwestern.edu/hoffman/endor_files/Simulation_programs.htm
ENDOR F2 ($S=\frac{1}{2}$)	1st order	[8], https://github.com/EndorF2/Simulation

ENDOR spectra. An arbitrary number of electron and nuclear spins can be treated by exact and 2nd order theory. *EasySpin* is available free of charge. Matlab version 7.5 or later must, however, be installed on the computer and is not provided with *EasySpin*.

EPR-NMR: This FORTRAN 77 program was written primarily for the handling of magnetic resonance spectra of single crystals and powders. It contains capabilities for NMR as well as EPR calculations and for handling of several unpaired electronic spins. The program sets up spin-Hamiltonian matrices and determines their eigenvalues using exact diagonalization.

Xemr: *Xemr* is an EPR, ENDOR, and TRIPLE spectrum manipulation and simulation package written for Linux systems. A numerical method can handle electron and nuclear Zeeman, hyperfine, electron–electron, and nuclear quadrupole interactions exactly in simulations of both EPR and ENDOR spectra. The program is distributed free of charge at <https://github.com/jmeloranta/xemr>.

XSophe-SOPHE: The *XSophe-Sophe-XeprView* computer simulation software suite is applicable for the analysis of isotropic, randomly oriented, and single crystal CW and pulse EPR spectra from isolated and clusters of paramagnetic centres. Spectra are simulated based on full matrix diagonalization.

Sim: Simulations were performed by diagonalization of the spin Hamiltonian used to model the complex under study. General Hamiltonians can be treated like exchange-coupled complexes of transition metal ions. Single crystal and powder spectra can be analysed. The software was developed by Dr Høgni Weihe, Department of Chemistry, University of Copenhagen.

MAGRES: *MAGRES* is a general program for the simulation of EPR, ENDOR and ESEEM spectra for any spin system in single crystals as well as in powders. The program can also be used for the calculation of NMR spectra. Exact diagonalization is used, hence no assumptions about the relative magnitudes of the interactions are made.

MSPEN: Powder-type EPR and ENDOR spectra were calculated by direct diagonalization of an appropriate spin Hamiltonian. Orientational selectivity was accounted for by a weighting function, later adopted in the ENDOR F2 program.

GENDOR: *GENDOR* is an ENDOR spectrum simulation program, combining data input and computation into a single Visual Basic program with a gui interface.

ENDORF2: *ENDORF2* is a Fortran77 program for the simulation of ENDOR spectra of free radicals in single crystals and powders, treating the *hfc*, *nqc* and nuclear Zeeman interactions as a joint perturbation [8–10]. Further information is available at <https://github.com/EndorF2/Simulation>.

References

- [1] G. Feher, Electronic structure of F centers in KCl by the electron spin double-resonance techniques, *Phys. Rev.* 105 (1957) 1122–1123.
- [2] R. Erickson, A. Lund, M. Lindgren, Analysis of powder EPR and ENDOR spectra of the biphenyl radical cation on H-ZSM-5 zeolite, silica gel and in CFCl_3 matrix, *Chem. Phys.* 193 (1–2) (1995) 89–99.
- [3] R. Erickson, N.P. Benetis, A. Lund, M. Lindgren, Radical cation of naphthalene on H-ZSM-5 zeolite and in CFCl_3 matrix. A theoretical and experimental EPR, ENDOR, and ESEEM study, *J. Phys. Chem. A* 101 (13) (1997) 2390–2396.
- [4] L.R. Dalton, A.L. Kwiram, ENDOR studies in molecular crystals. II. Computer analysis of the polycrystalline ENDOR spectra of low symmetry materials, *J. Chem. Phys.* 57 (1972) 1132–1145.
- [5] (a) R.B. Clarkson, R.L. Belford, K.S. Rothenberger, H.C. Crookham, ENDOR of perylene radicals adsorbed on alumina and silica-alumina powders. I. The ring protons, *J. Catal.* 106 (1987) 500–511; (b) K.S. Rothenberger, H.C. Crookham, R.L. Belford, R.B. Clarkson, ENDOR of perylene radicals adsorbed on alumina and silica-alumina powders: II. The matrix effects, *J. Catal.* 115 (1989) 430–440.
- [6] (a) R.B. Clarkson, K. Mattson, W. Shi, W. Wang, R.L. Belford, Electron Magnetic Resonance of Aromatic Radicals on Metal Oxide Surfaces, in: A. Lund, C. Rhodes (Eds.), *Radicals on Surfaces*, Kluwer, Dordrecht, 1995, pp. 89–117; (b) R.B. Clarkson, K. Mattson, W. Shi, W. Wang, R.L. Belford, Electron magnetic resonance of aromatic radicals on metal oxide surfaces, *Molecular Engineering* 4 (1994) 89–117.
- [7] (a) B.M. Hoffman, J. Martinsen, R.A. Venters, General theory of polycrystalline ENDOR patterns. g and hyperfine tensors of arbitrary symmetry and relative orientation, *J. Magn. Reson.* 59 (1984) 110–123; (b) B.M. Hoffman, R.A. Venters, J. Martinsen, General theory of polycrystalline ENDOR patterns. Effects of finite EPR and ENDOR component linewidths, *J. Magn. Reson.* 62 (1985) 537–542; (c) B.M. Hoffman, R.J. Gurbel, Polycrystalline ENDOR patterns from centers with axial EPR spectra. General formulas and simple analytic expressions for deriving geometric information from dipolar couplings, *J. Magn. Reson.* 82 (1989) 309–317.
- [8] R. Erickson, Simulation of ENDOR spectra of radicals with anisotropic hyperfine and nuclear quadrupolar couplings in disordered solids, *Chem. Phys.* 202 (1996) 263–275.
- [9] R. Erickson, Electron Magnetic Resonance of Free Radicals. Theoretical and Experimental EPR, ENDOR and ESEEM Studies of Radicals in Single Crystal and Disordered Solids, Linköping Studies in Science and Technology, PhD Thesis No. 391, ISBN 91-7871-582-2, Linköping, Sweden, 1995.
- [10] A. Lund, R. Erickson, EPR and ENDOR simulations for disordered systems: The balance between efficiency and accuracy, *Acta. Chem. Scand.* 52 (1998) 261–274.
- [11] C.P. Keijzers, E.J. Reijerse, P. Stam, M.F. Dumont, M.C.M. Grißnau, *MAGRES: A general program for electron spin resonance, ENDOR and ESEEM*, *J. Chem. Soc. Faraday Trans. 1* (83) (1987) 3493–3503.
- [12] A. Kreiter, J. Hüttermann, Simultaneous EPR and ENDOR powder spectra synthesis by direct Hamiltonian diagonalization, *J. Magn. Reson.* 93 (1991) 12–26.
- [13] M.J. Mombourquette, J.A. Weil, Simulation of magnetic resonance powder spectra, *J. Magn. Reson.* 99 (1992) 37–44.
- [14] G.R. Hanson, C.J. Noble, S. Benson, *XSophe-Sophe-XeprView and molecular sophe: computer simulation software suites for the analysis of continuous wave and pulsed EPR and ENDOR spectra*, in: A. Lund, M. Shiotani (Eds.), *EPR of free radicals in solids I, trends in methods and applications*, Springer, Dordrecht, 2013.
- [15] Stoll S. (2003) Spectral simulations in solid-state electron paramagnetic resonance. PhD thesis ETH 15059, Eidgenössische Technische Hochschule, Zürich.
- [16] S. Stoll, A. Schweiger, *EasySpin, a comprehensive software package for spectral simulation and analysis in EPR*, *J. Magn. Reson.* 178 (2006) 42–55.
- [17] EasySpin <http://www.easyspin.org/> Accessed 2020-10-27.
- [18] XEMR software package. <https://github.com/jmeloranta/xemr>. Accessed 2022-02-11.
- [19] J.H. Freed, Theory of multiple resonance and ESR saturation in liquids and related media, in: M.M. Dorio, J.H. Freed (Eds.), *Multiple Electron Resonance Spectroscopy*, Plenum Press, New York, 1979, pp. 73–142.
- [20] (a) M. Brustolon, T. Cassol, ENDOR Enhancements and relaxation properties of the $-\text{OOC}-\dot{\text{C}}\text{H}-\text{COO}-$ radical in a KH malonate single crystal, *J. Magn. Reson.* 60 (1984) 257–267; (b) M. Brustolon, T. Cassol, L. Micheletti, U. Segre, ENDOR studies of methyl dynamics in molecular crystals, *Mol. Phys.* 61 (1987) 249–255; (c) M. Brustolon, L. Maniero, U. Segre, An ENDOR study of the slow intramolecular motion in the $\text{CH}_2\text{COO}^\bullet$ radical, *Mol. Phys.* 65 (1988) 447–453.
- [21] (a) G.C. Hurst, T.A. Henderson, R.W. Kreilick, Angle-selected ENDOR spectroscopy. 1. Theoretical interpretation of ENDOR shifts from randomly orientated transition-metal complexes, *J. Am. Chem. Soc.* 107 (1985) 7294–7299; (b) T.A. Henderson, G.C. Hurst, R.W. Kreilick, Angle-selected ENDOR spectroscopy. 2. Determination of proton coordinates from a polycrystalline sample of bis(2,4-pentanedionato)copper (II), *J. Am. Chem. Soc.* 107 (1985) 7299–7303.
- [22] G.P. Gochev, N.D. Yordanov, Polycrystalline “ENDOR crystallography”, a new methodological approach, *J. Magn. Reson.* 102 (1993) 180–182.
- [23] A. Schweiger, H.S.H. Günthard, Transition probabilities in electron-nuclear double- and multiple-resonance spectroscopy with non-coherent and coherent radio-frequency fields, *Chem. Phys.* 70 (1982) 1–22.
- [24] M. Iwasaki, Second-order perturbation treatment of the general spin Hamiltonian in an arbitrary coordinate system, *J. Magn. Reson.* 16 (1974) 417–423.
- [25] (a) K.A. Thuomas, A. Lund, Analysis of EPR with large quadrupole interaction, *J. Magn. Reson.* 22 (1976) 315–325; (b) A. Lund, K.A. Thuomas, J. Mariani, Calculation of powder ESR spectra of radicals with hyperfine and quadrupolar interactions. Application to mono- and dichloroalkyl radicals *J. Magn. Reson.* 30 (1978) 505–514.

- [26] R. Lefebvre, J. Maruani, Use of computer programs in the interpretation of electron paramagnetic resonance spectra of dilute radicals in amorphous solid samples. 1. High field treatment. X-band spectra of π -electron unconjugated hydrocarbon radicals, *J. Chem. Phys.* 42 (1965) 1480–1496.
- [27] (a) C.J. Bender, M. Sahlin, G.T. Babcock, B.A. Barry, T.K. Chandrasekar, S.P. Salowe, J. Stubbe, B. Lindström, L. Pettersson, A. Ehrenberg, B.M. Sjöberg, An ENDOR study of the tyrosyl free radical in ribonucleotidoreductase from *Escherichia coli*, *J. Am. Chem. Soc.* 111 (1989) 8076–8083; (b) C. Tommos, X.-S. Tang, K. Warncke, C.W. Hoganson, S. Styring, J. McCracken, B.A. Diner, G.T. Babcock, Spin-density distribution, conformation, and hydrogen bonding of the redoxactive tyrosine YZ in photosystem II from multiple-electron magnetic-resonance spectroscopies, *J. Am. Chem. Soc.* 117 (1995) 10325–10335.
- [28] K. Toriyama, K. Nunome, M. Iwasaki, ENDOR studies of methyl radicals in irradiated single crystals of $\text{CH}_3\text{COOLi}\cdot 2\text{H}_2\text{O}$, *J. Chem. Phys.* 64 (1976) 2020–2026.
- [29] K. Möbius, W. Lubitz, ENDOR spectroscopy in photobiology and biochemistry, in: L.J. Berliner, J. Reuben (Eds.), *Biological Magnetic Resonance*, Vol 7, Plenum Press, New York, 1987.
- [30] D.H. Whiffen, ENDOR transition moments, *Mol. Phys.* 10 (1966) 595–596.
- [31] M. Fujimoto, C.A. McDowell, T.J. Takui, Ligand ENDOR spectra of Cu(II) impurity complexes in α -glycine crystals, *Chem. Phys.* 70 (1979) 3694–3701.
- [32] P. Kottis, R. Lefebvre, Calculation of the electron spin resonance line shape of randomly oriented molecules in a triplet state. I. The $\Delta m = 2$ transition with a constant linewidth, *J. Chem. Phys.* 39 (1963) 393–403.
- [33] M. Iwasaki, K. Toriyama, K. Nunome, E.s.r. evidence for the static distortion of $^2\text{E}_{1g}$ benzene cations giving $^2\text{B}_{2g}$ with D_{2h} symmetry in low temperature matrices, *J. Chem. Soc., Chem. Commun.* 6 (1983) 320–322.
- [34] H.M. McConnell, J. Strathdee, Theory of anisotropic hyperfine interactions in π -electron radicals, *Mol. Phys.* 2 (1959) 129–138.
- [35] a) M.B. Huang, S. Lunell, Accurate configuration interaction calculations of the hyperfine interactions in the benzene cation, *J. Chem. Phys.* 92 (1990) 6081–6083. b) S. Lunell, J.W. Gauld, R.M. Kadam, Y. Itagaki, A. Lund, Theoretical and Experimental Studies of the Benzene Radical Cation: Effects of Selective Deuteration, *Adv. Quantum Chem.* 35 (1995) 339–355.
- [36] (a) R.M. Kadam, R. Erickson, K. Komaguchi, M. Shiotani, A. Lund, ENDOR and EPR studies of benzene radical cations in halocarbon matrices: the static Jahn–Teller distortion of the monomer and geometry of the dimer cation, *Chem. Phys. Lett.* 290 (1998) 371–378; (b) R.M. Kadam, Y. Itagaki, R. Erickson, A. Lund, ENDOR and ESR studies of radical cations of methyl-substituted benzene in halocarbon matrices, *J. Phys. Chem. A* 103 (1999) 1480–1486; (c) R.M. Kadam, Y. Itagaki, N.P. Benetis, A. Lund, R. Erickson, W. Hilczler, An EPR, ENDOR and ESEEM study of the benzene radical cation in CFCl_3 matrix: isotopic substitution effects on structure and dynamics, *PCCP*, 1 (1999) 4967–4974; (d) Y. Itagaki, R.M. Kadam, A. Lund, N.P. Benetis, Structure of dimeric cations of benzene and toluene in halocarbon matrices: ESR, ENDOR and MO studies, *PCCP* 2 (2000) 2683–2688.
- [37] V.I. Feldman, F. Sukhov, A. Orlov, R. Kadam, Y. Itagaki, A. Lund, Effect of matrix and substituent on the electronic structure of trapped benzene radical cations, *Phys. Chem. Chem. Phys.* 2 (2000) 29–35.
- [38] a) F. Gerson, X.-Z. Qin, The radical cation of naphthalene: first correct analysis of its ESR spectrum, *Chem. Phys. Lett.* 153 (1988) 546–550. b) F. Gerson, Applications of ENDOR spectroscopy to radical cations in freon matrices, *Accounts Chem. Res.* 27 (1994) 63–69.
- [39] O. Edlund, P.O. Kinell, A. Lund, A. Shimizu, Electron spin resonance spectra of monomeric and dimeric cations of benzene, *J. Chem. Phys.* 46 (1967) 3679.
- [40] Y. Itagaki, N. Yanagida, M. Shiotani, Formation and structure of dimer radical cations of fluorinated benzenes in solid matrices, *Phys. Chem. Chem. Phys.* 4 (2002) 5982–5987.
- [41] A.F. Bedilo, A.M. Volodin, Radical cations of aromatic molecules with high ionization potentials on the surfaces of oxide catalysts: Formation, properties, and reactivity, *Kinet. Catal.* 50 (2009) 314–324.
- [42] E. Sagstuen, E.O. Hole, S.R. Haugedal, W.H. Nelson, Alanine radicals: Structure determination by EPR and ENDOR of single crystals X-irradiated at 295 K, *J. Phys. Chem. A* 101 (1997) 9763–9772.
- [43] M.Z. Heydari, E. Malinen, E.O. Hole, E. Sagstuen, Alanine radicals. 2. The composite polycrystalline alanine EPR spectrum studied by ENDOR. Thermal annealing and spectrum simulations, *J. Phys. Chem. A* 106 (2002) 8971–8977.
- [44] R. LoBrutto, Y.H. Wei, R. Mascarenhas, C.P. Scholes, T.E. King, Electron nuclear double resonance and electron paramagnetic resonance study on the structure of the NO-ligated heme alpha 3 in cytochrome c oxidase, *J. Biol. Chem.* 258 (1983) 7437–7448.
- [45] V.P. Chacko, C.A. McDowell, B.C. Singh, ^{14}N and ^1H ENDOR studies of X-irradiated single crystals of hippuric acid, *J. Chem. Phys.* 72 (1980) 4111–4116.
- [46] N.A. Salih, A. Sanderud, E. Sagstuen, O.I. Eid, A. Lund, ESR, ENDOR and FSE studies of hippuric acid single crystals X-irradiated at 195 K: A reinvestigation, *J. Phys. Chem. A* 101 (1997) 8214–8220.
- [47] R. Erickson, A. Lund, Applications of EPR and ENDOR Spectrum simulations in radiation research in A. Lund, M. Shiotani (Eds.) *Applications of EPR in Radiation Research*, Springer, 2014.
- [48] K. Komaguchi, Y. Matsubara, M. Shiotani, H. Gustafsson, E. Lund, A. Lund, An ESR and ENDOR study of irradiated Li-6-formate, *Spectrochim. Acta A* 66 (2007) 754–760.
- [49] T.A. Vestad, H. Gustafsson, A. Lund, E.O. Hole, E. Sagstuen, Radiation-induced radicals in lithium formate monohydrate ($\text{LiHCO}_2 \cdot \text{H}_2\text{O}$). EPR and ENDOR studies of X-irradiated crystal and polycrystalline samples, *Phys. Chem. Chem. Phys.* 6 (2004) 3017–3022.
- [50] G.H. Rist, J.S. Hyde, Ligand ENDOR of metal complexes in powders, *J. Chem. Phys.* 52 (1970) 4633–4643.
- [51] H. Li, D. Biglino, R. Erickson, A. Lund, The structure of a copper(II) complex with water in Cu-ZSM-5 at 4 K by ENDOR, *Chem. Phys. Lett.* 266 (1997) 417–421.
- [52] D. Biglino, H. Li, R. Erickson, A. Lund, H. Yabiro, M. Shiotani, EPR and ENDOR studies of NO_x and Cu^{2+} in zeolites: bonding and diffusion, *PCCP* 1 (1999) 2887–2896.
- [53] M.W. Anderson, L. Kevan, Study of Cu^{2+} -doped zeolite NaH-ZSM-5 by electron spin resonance and electron spin echo modulation spectroscopies, *J. Phys. Chem.* 91 (1987) 4174–4179.
- [54] R. Erickson, A. Lund, Analytical expressions of magnetic energies and wavefunctions of paramagnetic systems with $S=1/2$ and $I=1$ or $I=3/2$, *J. Magn. Reson.* 92 (1991) 146–151.
- [55] N.M. Atherton, *Principles of electron spin resonance*, Ellis Horwood and PTR Prentice Hall, Physical Chemistry Series, Ellis Horwood, Chichester, 1993.
- [56] G.S. Owen, G. Vincow, Computer simulation of the ESR spectra of the naphthalene, anthracene, and perylene radical cations in a polycrystalline medium, *J. Chem. Phys.* 54 (1971) 368–375.
- [57] I.C. Lewis, L.S. Singer, Electron spin resonance of radical cations produced by the oxidation of aromatic hydrocarbons with SbCl_5 , *J. Chem. Phys.* 43 (1965) 2712–2727.
- [58] T. Bally, C. Carra, M.P. Fülcher, Z. Zhu, Electronic structure of the naphthalene radical cation and some simple alkylated derivatives, *Chem. Soc. Perkin Trans. 2* (1998) 1759–1765.
- [59] J.L. Courtneidge, A.G. Davies, T. Clark, D. Wilhelm, The electron spin resonance spectrum of the biphenyl radical cation, *J. Chem. Soc. Perkin Trans. 1* (1984) 1197–1200.
- [60] W.A. Bernhard, The use of alpha hyperfine coupling tensors as a measure of unpaired spin density and free radical geometry, *J. Chem. Phys.* 81 (1984) 5928–5936.